PNAS RESEARCH ARTICLE | EARTH, ATMOSPHERIC, AND PLANETARY SCIENCES

Cloud microphysical response to entrainment and mixing is locally inhomogeneous and globally homogeneous: Evidence from the lab

Jae Min Yeom[a,1], Ian Helman[a], Prasanth Prabhakaran[a,b], Jesse C. Anderson[a], Fan Yang[c], Raymond A. Shaw[a,1], and Will Cantrell[a,1]

Edited by Richard Rotunno, National Center for Atmospheric Research, Boulder, CO; received May 4, 2023; accepted September 11, 2023

Entrainment of dry air into clouds strongly influences cloud optical and precipitation properties and the response of clouds to aerosol perturbations. The response of cloud droplet size distributions to entrainment–mixing is examined in the Pi convection-cloud chamber that creates a turbulent, steady-state cloud. The experiments are conducted by injecting dry air with temperature (T_e) and flow rate (Q_e) through a flange in the top boundary, into the otherwise well-mixed cloud, to mimic the entrainment–mixing process. Due to the large-scale circulation, the downwind region is directly affected by entrained dry air, whereas the upwind region is representative of the background conditions. Droplet concentration (Cn) and liquid water content (L) decrease in the downwind region, but the difference in the mean diameter of droplets (D_m) is small. The shape of cloud droplet size distributions relative to the injection point is unchanged, to within statistical uncertainty, resulting in a signature of inhomogeneous mixing, as expected for droplet evaporation times small compared to mixing time scales. As T_e and Q_e of entrained air increase, however, Cn, L, and D_m of the whole cloud system decrease, resulting in a signature of homogeneous mixing. The apparent contradiction is understood as the cloud microphysical responses to entrainment and mixing differing on local and global scales: locally inhomogeneous and globally homogeneous. This implies that global versus local sampling of clouds can lead to seemingly contradictory results for mixing, which informs the long-standing debate about the microphysical response to entrainment and the parameterization of this process for coarse-resolution models.

cloud microphysics | entrainment | homogeneous vs. inhomogeneous mixing

Significance

Cloud properties depend strongly on their response to the entrainment and mixing of environmental air into the cloud. In one limit (inhomogeneous mixing), droplet growth can be accelerated due to the diminished number of droplets that compete for the available water vapor. We investigate the response of cloud droplet sizes to entrainment in clouds formed in the laboratory. They respond to the entrainment and mixing differently depending on the time scales: locally inhomogeneous and globally homogeneous. The apparent contradiction results from the system residing in multiple equilibrium states, and this helps inform the longstanding debate about the type of mixing that occurs in natural clouds.

Marine boundary-layer clouds cover large regions of the globe and are known to strongly influence radiative balances. The microphysical properties and persistence of these clouds are dramatically affected by cloud-top entrainment and turbulent mixing within the cloud layer. However, the impact of entrainment and turbulent mixing on cloud microphysical properties is still poorly understood. This paper addresses the microphysical response to entrainment based on experiments performed in the Pi Convection-Cloud Chamber. In these experiments, we observe the effects of warm, dry air that is entrained and mixed into a turbulent cloud, pre-existing in the chamber. These laboratory experiments have two advantages: 1) the boundary conditions are known, and the entrainment rate is varied in a controlled way so that the cloud microphysical response can be observed; 2) the experiments take place in a dynamic steady state, such that the inherently transient entrainment–mixing process can be explored in detail through extended sampling at multiple Eulerian points relative to the entrainment zone; 3) complicating feedbacks are minimized because of the controlled conditions, thereby allowing mechanisms to be clearly identified so that they can later be explored in more complex environments, e.g., through fully coupled computational models. Ultimately, the goal is to understand the microphysical response to entrainment and turbulent mixing in detail so that it can inform the community's explorations of extensive, long-lived stratocumulus clouds.

Previous laboratory investigations of entrainment relevant to clouds have been few in number, but have played an important role in clarifying mechanisms. Most notably, Latham and Reed (1) conducted experiments to investigate the effects of mixing of unsaturated air on the droplet size distribution. They found that the mixing process was highly inhomogeneous. Shy and Breidenthal (2, 3) explored the phenomenon of buoyancy reversal and its contribution to the cloud-top entrainment instability mechanism previously proposed by Randall (4) and Deardorff (5). They found that even for relatively large buoyancy reversal parameters, the entrainment interface was stable. Indeed, as summarized by Siems et al. (6), rather than destabilizing an entire cloud layer as originally envisioned, "buoyancy reversal leads to weak circulations rather reminiscent of Rayleigh–Bénard convection in the lower layer." These laboratory experiments were influential in placing

Author affiliations: [a]Department of Physics and Atmospheric Sciences Program, Michigan Technological University, Houghton, MI 49931; [b]Cooperative Institute for Research in Environmental Sciences, University of Colorado Boulder Chemical Sciences Lab, National Oceanic and Atmospheric Administration, Boulder, CO 80309; and [c]Brookhaven National Laboratory, Upton, NY 11973

Author contributions: J.Y., P.P., F.Y., R.A.S., and W.C. designed research; J.Y., I.H., P.P., and J.C.A. performed research; J.Y., R.A.S., and W.C. analyzed data; and J.Y., I.H., P.P., J.C.A., F.Y., R.A.S., and W.C. wrote the paper.

The authors declare no competing interest.

This article is a PNAS Direct Submission.

[1]To whom correspondence may be addressed. Email: jyeom2@mtu.edu, rashaw@mtu.edu, or cantrell@mtu.edu.

This article contains supporting information online at https://www.pnas.org/lookup/suppl/doi:10.1073/pnas.2307354120/-/DCSupplemental.

Published October 9, 2023.

buoyancy reversal in its proper context for stratocumulus cloud circulations, and in the recognition that cloud-top entrainment instability plays a relatively minor role in the atmosphere. Sayler and Breidenthal (7) extended the laboratory investigations of entrainment at a stable interface and demonstrated the significant role of cloud top cooling for driving cloud-scale circulations.

In contrast to previous studies, this investigation focuses on how entrainment influences cloud microphysical properties within the extreme limits of perfectly homogeneous and inhomogeneous mixing. Specifically, given that liquid water content, L, is proportional to the product of droplet number concentration and mean volume of droplets, the entrainment of dry air can lead to a uniform reduction of all droplet radii (homogeneous mixing), or a reduction of the droplet number concentration and fixed droplet size (inhomogeneous mixing), or somewhere in between those limits. Due to complete evaporation of some droplets, inhomogeneous mixing can promote subsequent growth of cloud droplets and lead to a significant broadening of the size distribution, which may help explain the gap between observation and theory. Field observations have been confounding, seemingly indicating that different mixing types are possible (8–15). More recently, Desai et al. (16) and Yeom et al. (17) found evidence that mixing tends to be more inhomogeneous near cloud top and becomes increasingly homogeneous with increasing depth into the cloud. Numerical studies, e.g., typical large eddy simulations of stratocumulus clouds, are not able to provide reliable guidance because of their coarse resolution and the implicit assumption that droplets in one grid box experience the same supersaturation. Implementation of efficient linear eddy models for subgrid representation of turbulent mixing indicates that inhomogeneous mixing can play an important role in driving the microphysical properties within stratocumulus clouds (18). That progress is based on earlier work using linear eddy models coupled with droplet growth and evaporation to explore mixing scenarios (19).

The approach of this work, therefore, is to implement an entrainment flow in the Pi Chamber, with known mass flow rate, temperature, and relative humidity (RH), and to monitor the cloud droplet size distribution in different spatial locations relative to the entrainment region. We then interpret the observed size distributions in the context of homogeneous versus inhomogeneous mixing. A convenient aspect of the implementation is the existence of a large-scale circulation (LSC), which is closely linked to the turbulent energy dissipation rate in the convection-cloud chamber (20, 21). This results in shear at the entrainment interface and also allows the experiments to be conveniently performed at positions ranging from upstream to downstream of the entrainment region.

We begin by introducing the experiment setup in more detail and then present results, including interpretation of the observations in scalar flux budget model and relevant time scales. Finally, we discuss the results in the context of atmospheric clouds and share concluding remarks.

Results

Experiment Set-Up. The laboratory facility, the Pi Chamber, has been described in detail in previous publications (22). Here, we cover only the basic outline and modifications to the typical operation, which enables the entrainment experiments. A cloud is created in the chamber through a temperature gradient between warm and cool water-saturated top and bottom surfaces. One of the key advantages of the chamber is that the mixing cloud thus created can be sustained in steady state for hours at a time. Steady-state cloud conditions are achieved when the source of cloud droplets from aerosol injected into the chamber is balanced by subsequent removal of cloud droplets due to gravitational settling.

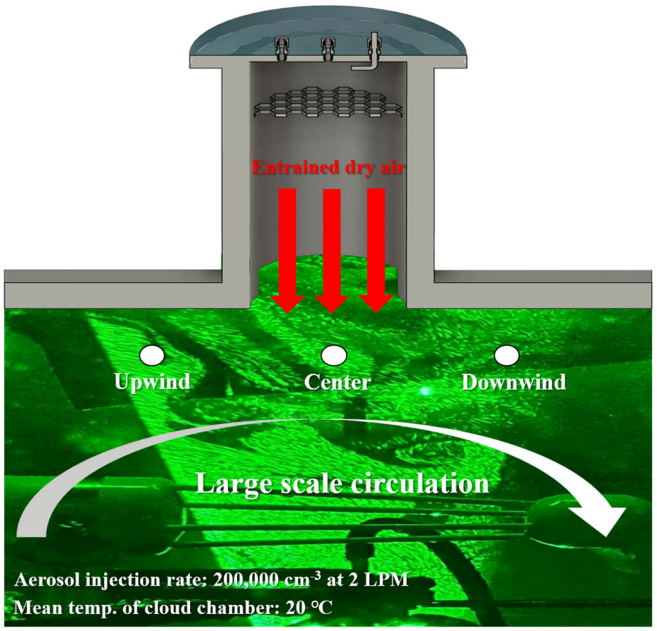

Fig. 1. An overview of the experimental approach, showing a photograph of the turbulent cloud illuminated by a laser light sheet. The temperatures of the top, wall, and bottom surfaces are set to 15 °C, 20 °C, and 25 °C, respectively, resulting in a temperature gradient of ΔT = 10 K and a mean temperature of 20 °C. NaCl particles, size selected at 130 nm using an Aerodynamic Aerosol Classifier (AAC), are injected at a constant rate (200,000 cm^{-3} at 2 LPM). The cross-sectional view of the top cylinder (called "flange") and the upper part of the chamber is shown. A flow straightener is installed inside the flange to make the flow laminar (marked as red arrows). Filaments of dry air come from the bottom of the flange, visible just below the bright streak. The direction of LSC in the chamber is shown schematically with the curved arrow. Following the direction of LSC, the cloud droplet size distributions are measured at three different regions (upwind, center, and downwind regions of the entrainment zone).

In this study, we modified the basic setup to mimic the entrainment–mixing process occurring, for example, at the top of stratocumulus clouds or the edge of cumulus clouds. In essence, we create a steady-state cloud in the main portion of the chamber, then inject dry, particle-free air from the top, through a temperature-controlled flange. See Fig. 1 for a schematic of the flange and the region immediately below it. The flange is designed so that the air flow is humidity and temperature controlled, and a flow straightener ensures that the flow is laminar.

In the experiments presented here, the temperatures of the top, sidewall, and bottom surfaces of the main portion of the chamber are set to 15 °C, 20 °C, and 25 °C, resulting in an unstable temperature difference of ΔT = 10 K and a mean temperature of 20 °C. The experiments start with cloudy Rayleigh–Bénard convection conditions for a few hours to ensure steady state. Once steady-state cloud conditions have been achieved, air with temperatures of 20 °C and 30 °C and 65% RH is injected into the cloudy region through the entrainment zone with two constant flow rates, 5 and 20 liters per minute (LPM), respectively. These flow rates correspond to entrainment velocities of 0.37 and 1.5 cm s^{-1}, which are comparable to the values in the real atmosphere (23, 24). Compared to the experiment without entrainment, the cloud microphysical properties reach very different steady-state conditions depending on the properties of the entrained air. The entrained air does not contain aerosol particles, so the effect of secondary droplet activation due to the entrained air is negligible; exploring that variable will be the focus of future work.

For these experiments, the LSC takes the form of a single roll with a preferred orientation. Following the direction of the LSC,

we installed a traverse in the chamber such that we could measure cloud droplet distributions with a Welas-2000 optical particle counter covering 0.583- to 40.679-μm diameter range in the upwind, center, and downwind regions of the entrainment zone. The downwind region is directly affected by entrained air from the entrainment zone, whereas the upwind region represents the background conditions in the cloud chamber (Fig. 1). For statistical significance, five samples are obtained at each measurement position for each steady-state condition achieved by different entrained air properties, such as entrained air temperature and flow rate, and each sample is measured for 50 s. In separate experiments in dry conditions (i.e., no cloud present in the chamber), we measured the temperature with a thermistor to verify that these regions do indeed represent background and entrainment-influenced conditions. (See *SI Appendix* for further details.)

Cloud Microphysical Properties for Different Conditions. Fig. 2 *A* and *B* show the nonnormalized and normalized mean cloud droplet size distributions for each region under the entrained air temperature T_e = 30 °C and flow rate Q_e = 20 LPM. The cloud droplet number concentration (Cn) in the downwind region decreases significantly compared to the center and upwind regions (Fig. 2*A*). The reduction of Cn is most striking at the highest T_e and Q_e conditions because the evaporation of droplets is more efficient, and this reduction tends to be smaller as T_e and Q_e decrease. The important thing to note is that the shapes of droplet size distributions for the three regions are essentially the same when normalized, regardless of the entrained air conditions. This is consistent with the inhomogeneous mixing hypothesis: Complete evaporation of the droplets at the interfacial region between cloudy and entrained dry air occurs first, followed by mixing between saturated air and cloudy air with little change in the shape of droplet size distribution.

We now investigate how the entrained air affects the whole cloud chamber system depending on its conditions. The comparison of each normalized droplet size distribution at the downwind location for different conditions of entrained air is shown in Fig. 2*C*. Compared to the baseline droplet size distribution that represents the result from the experiment without entrainment, the droplet size distributions are shifted to smaller sizes and become slightly narrower as T_e and Q_e increase. The droplet size distributions from the other two regions (center and upwind) show the same tendency, as shown in Fig. 2*C* (*SI Appendix*, Fig. S2). The averages of cloud microphysical variables [Cn, liquid water content (L), and mean diameter of droplets (D_m)] for all four different entrained air conditions and base condition without entrainment are summarized in *SI Appendix*, Table S1. It clearly shows the characteristics described above.

Although visually evident, it is important to test the statistical significance of the inhomogeneous and homogeneous signatures (*SI Appendix* for further details). The Kolmogorov–Smirnov (KS) test is used to determine whether two distributions from different

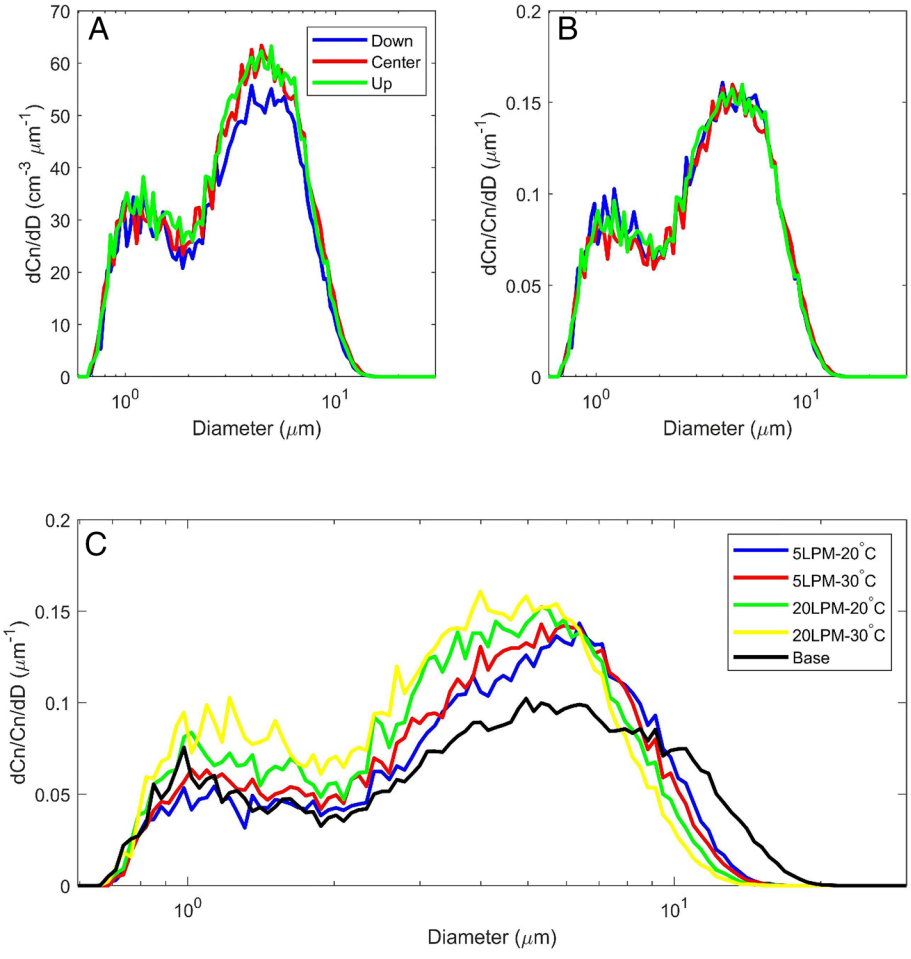

Fig. 2. (*A*) The nonnormalized and (*B*) normalized mean cloud droplet size distributions at each measurement point (downwind, center, and upwind) under one specific entrained air condition (flow rate Q_e = 20 LPM and temperature T_e = 30 °C). (*C*) The comparison of each normalized droplet size distribution at the downwind location for all four different entrained air conditions (5 LPM-20 °C, 5 LPM-30 °C, 20 LPM-20 °C, and 20 LPM-30 °C) and base condition (without entrainment).

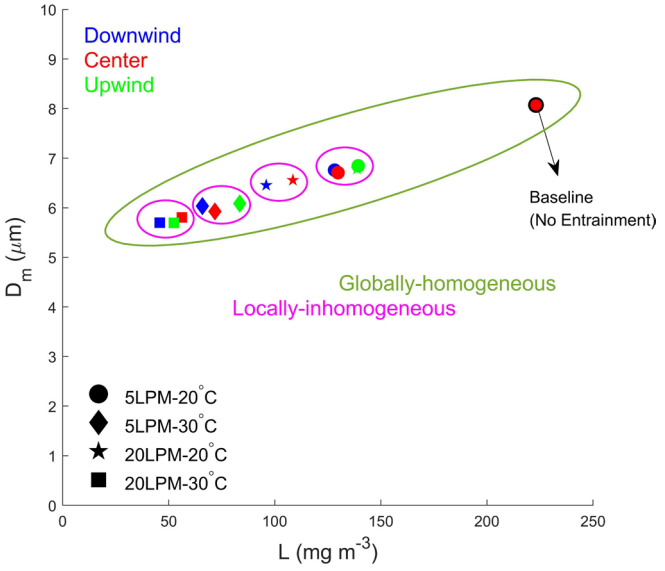

Fig. 3. The relationships between liquid water content (L) and mean diameter (D_m) of droplets for all experiments illustrate the local versus global effects of entrained air. The uncertainties of L and D_m are about 10 mg m^{-3} and 0.1 μm, respectively. Note that the point of 5 LPM-30 °C experiments in the upwind region overlaps with the point of 5 LPM-20 °C experiments in the upwind region.

regions (e.g., downwind and center) are from the same parent distribution. Under the same experimental condition, the results from the KS test show that the distribution shapes between the two regions are not different at the 5% significance level, which is consistent with the dominant observed inhomogeneous mixing feature. *t* tests are also conducted for three cloud microphysical variables (Cn, L, and D_m) for different experiments at the same sampling location. Most results from this test are rejected at the 5% level, which means that the microphysical values from different experiments are statistically different, as shown in *SI Appendix*, Table S4, and as is qualitatively evident in Fig. 2*C*.

The relationships between L and D_m for all experiments illustrate the effects of entrained air at different locations and also for different entrainment conditions (Fig. 3). The differences between each region under the same entrained air condition represent what we refer to as the "local" effects of the entrained air, whereas the differences between the four entrained air conditions indicate what we refer to as the "global" effects on the whole cloud system. The local effects of entrained air are evident within each cluster of data points. L is always the smallest in the downwind region for each experiment because this region is directly affected by entrained air, but D_m is almost the same between these three regions. The reduction of L is mainly caused by the complete evaporation of droplets, which suggests inhomogeneous mixing. From the system point of view, the relationship between L and D_m is clearly positive, which is indicative of homogeneous mixing. As T_e and Q_e increase, L and D_m of the whole cloud system continue to decrease. These two results showing locally inhomogeneous and globally homogeneous mixing traits are striking and beg for further interpretation.

Scalar Flux-Budget Analysis. From the analysis of cloud microphysical properties for each imposed entrainment condition, we expect that the clouds reach different steady-state thermodynamic and microphysical properties because the supersaturation field derived from T and water vapor mixing ratio, q_v, is also changed due to the entrained air. However, the exact measurement of supersaturation is challenging, so a scalar flux budget is used to estimate the mean supersaturation with different entrainment conditions. Such fundamental calculations are helpful in understanding why the clouds have different steady-state microphysical properties.

The heat flux equation for T with areas of the top, bottom, and sidewalls (A_t, A_b, and A_s) is given by

$$\frac{(T_{t,b,s} - T)\kappa}{\lambda} A_{t,b,s} = \rho C_p \frac{dT}{dt} V,$$

where $T_{t,b,s}$ are the temperatures of the top, bottom, and sidewalls; $T\left(= T_t + T_b/2\right)$ is the mean temperature when well mixed; λ, κ, ρ, C_p, and V are the thickness of boundary layer, thermal conductivity of air, density of air, specific heat of air, and volume, respectively. The time scale for each area (τ_t, τ_b, and τ_s) can be calculated as

$$\tau_{t,b,s} = \frac{\lambda V}{\alpha A_{t,b,s}},$$

where α is thermal diffusivity. Additionally, the term of entrainment flux is added in our experimental scenario. The time scale for this term (τ_e) can be written as

$$\tau_e = \frac{mass\ of\ air\ in\ chamber}{mass\ rate\ from\ entrainment}.$$

The differential equation for the time rate of change of temperature in the chamber is then,

$$\frac{dT}{dt} = \frac{(T_t - T)}{\tau_t} + \frac{(T_b - T)}{\tau_b} + \frac{(T_e - T)}{\tau_e} + \frac{(T_s - T)}{\tau_s},$$

For q_v, a similar equation can be written. Therefore, the steady-state conditions of T and q_v in the chamber with the entrainment flange from the above equations are given by

$$T = \left(\frac{T_t}{\tau_t} + \frac{T_b}{\tau_b} + \frac{T_e}{\tau_e} + \frac{T_s}{\tau_s}\right) \cdot \left(\frac{1}{\tau_t} + \frac{1}{\tau_b} + \frac{1}{\tau_e} + \frac{1}{\tau_s}\right)^{-1},$$

and

$$q = \left(\frac{q_t}{\tau_t} + \frac{q_b}{\tau_b} + \frac{q_e}{\tau_e} + \frac{q_s}{\tau_s}\right) \cdot \left(\frac{1}{\tau_t} + \frac{1}{\tau_b} + \frac{1}{\tau_e} + \frac{1}{\tau_s}\right)^{-1}.$$

With the assumption of saturated sidewalls, the maximum supersaturation achieved under a given condition can be calculated as a function of entrained air conditions. The important point is that the values of supersaturation calculated here are in the cloud-free condition (no cloud droplets), not the in-cloud condition. We explore the variations of supersaturation depending on the RH of entrained air under different entrainment conditions (*SI Appendix*, Fig. S3). For the calculation, the top, sidewall, and bottom temperatures are the same as in the experimental setup. The supersaturation can reach 2.29% without the entrainment. However, it varies significantly depending on the properties of entrained air. The values of supersaturation decrease monotonically as Q_e and T_e increase: the supersaturations are 2.26% with T_e = 20 °C and Q_e = 5 LPM; 2.26% with T_e = 30 °C and Q_e = 5 LPM; 2.19% with T_e = 20 °C and Q_e = 20 LPM; and 2.16% with T_e = 30 °C and Q_e = 20 LPM conditions when the RH of the entrained air is assumed to be 65%. The liquid water content is expected to respond to the variations in cloud-free supersaturation. Indeed, there is a decreasing trend for the normalized droplet size distributions for five experiments with different entrainment conditions: the values of L and D_m for these experiments decrease in the same order as the estimated supersaturations. This analysis

indicates that the clouds under different entrainment conditions have different steady-state cloud properties due to the change in the supersaturation field. The sidewalls in the experiment could be slightly subsaturated because the water vapor source of the sidewalls is only from the condensation of droplets on the walls. However, the decreasing trend is the same because the supersaturation is just scaled down if sidewalls are subsaturated. Although the saturation calculated from this model might not be exact, it can explain why the decreasing trend was observed, and it indicates a homogeneous mixing response.

Time Scale Analysis. To make a connection to the microphysical results in the above sections, we now explore whether the relevant time scales can account for the local and system-wide effects of entrained air. Previous studies have established the Damköhler number (Da = τ_{mix}/τ_{evap}) as an important parameter governing whether the mixing is homogenous or inhomogeneous, where τ_{mix} is the turbulent mixing time scale and τ_{evap} is the evaporation time scale (25–27). τ_{mix} represents the time needed to homogenize a volume of a linear size L through turbulent mixing and can be given by

$$\tau_{\text{mix}} = \left(\frac{L^2}{\varepsilon}\right)^{1/3},$$

where ε is the eddy dissipation rate of turbulent kinetic energy. In our experiments, L is assumed to be 13.5 cm, considering the distance from the center to the downwind region. The frequency of the LSC was approximately constant, with a mean frequency of 1.24×10^{-2} Hz and a range from 1.22×10^{-2} to 1.27×10^{-2} Hz. Using the relationship in Neidermeier et al. (20) the frequency of the LSC being constant means the bulk average ε is also constant (~10 $cm^2\ s^{-3}$). Therefore, τ_{mix} ~ 3 s is obtained from these experiments. τ_{evap}, which is the time needed for a population of droplets with a mean diameter to evaporate in subsaturated conditions, can be calculated as

$$\tau_{\text{evap}} = -\frac{{D_m}^2}{4\xi s},$$

where ξ is a function of air pressure and temperature and s is the supersaturation. The phase relaxation time scale (τ_{phase}), which is the time needed to restore saturation, can also be of relevance to the microphysical response, but in this case τ_{phase} ~ 1 to 3 s, approximately a factor of 10 greater than τ_{evap} (~0.1 s). Lehmann et al. (8) suggested the reaction time scale (τ_{react}) to consider the interactive changes of the saturation ratio and droplet size during the evaporation of droplets in a mixed volume. It is defined as the time either when the droplets are evaporated completely or when the saturation ratio approaches unity (they took when it reaches 0.995). In our case, τ_{react} is about 0.1 s, which means that τ_{evap} is dominant due to the low humidity of entrained air. The values of two characteristic time scales for the four experiments are shown in Table 1. Significantly, the values of τ_{evap} are much smaller than τ_{mix}, so the mixing region has high values of Da (~25) in all four conditions. Additionally, τ_{evap} is much less than the time (>3 s) required for the air to move from the upwind to downwind regions considering the distance between upwind and downwind regions and the velocity of LSC (a few cm s^{-1}). According to the accepted understanding of cloud microphysical response to mixing, Da ≫ 1 indicates the prevalence of extreme inhomogeneous mixing. It is consistent with the fact that the shapes of normalized droplet size distributions are always the same regardless of the entrained air conditions (Fig. 2*B*). Therefore, the local (immediate) effect of entrained air seems indeed to be dominantly inhomogeneous.

Table 1. Time scales for the four experiments

Experiments	τ_{evap} (s)	τ_{mix} (s)
5 LPM-20°C	0.13	2.63
5 LPM-30°C	0.12	2.63
20 LPM-20°C	0.10	2.63
20 LPM-30°C	0.09	2.63

We expect that the supersaturation adjusts to different entrained air conditions, as suggested by the scalar flux budget model. To quantitatively evaluate this hypothesis, we consider a time scale for the system (τ_{sys}),

$$\tau_{\text{sys}} = \left(\frac{1}{\tau_t} + \frac{1}{\tau_b} + \frac{1}{\tau_e} + \frac{1}{\tau_s}\right)^{-1},$$

the harmonic mean of the boundary flux time scales (τ_t, τ_b, τ_e, and τ_s). It can be interpreted as the time needed for the system to relax to an equilibrium state for given, constant boundary fluxes. In our experiments, the estimated value of τ_{sys} is about 25 s. It is much longer than τ_{mix} (~3 s), implying that the entrained air mixes completely with cloudy air before turning over within the chamber. Because the entrainment flow is maintained for times much longer than the system time scale or any of the relevant mixing or microphysical time scales, each set of experiments can be considered as being in steady state. The clouds with different steady-state microphysical properties can be considered individual cloud parcels affected by different properties of entrained air and provide insight into how the clouds respond to the influence of entrained air.

Atmospheric Implications: Local versus Global. From the global point of view, the system response time for the whole chamber (i.e., the characteristic time needed for the chamber to reach a new steady state for a given entrainment rate) is much larger than the local mixing time scale (~3 s). On the other hand, the microphysical response time, which is controlled by evaporation of droplets in a local environment, is similar as before (~1 s or less). Therefore, we would expect that a Da number defined for the whole chamber would be even larger than the local Da number, suggesting the microphysical response would also be inhomogeneous globally. However, chamber observations (Fig. 3) indicate that the system has an apparent globally homogeneous behavior between different entrainment events. So how to explain this apparent contradiction? The resolution is shown schematically in Fig. 4, where we depict the convection-cloud chamber with two different entrainment fluxes E_1 and E_2. Within each chamber depicted in the schematic, the mixing is inhomogeneous; in other words, the droplet size distribution observed at points upstream and downstream of the entrainment region shows a reduction in the droplet concentration but with the shape of the droplet size distribution unchanged. This is what we refer to as local behavior. Now we consider that the entrainment flux is changed from E_1 to E_2, such that the system slowly evolves to a new steady state, starting with a liquid water content of L_1 and adjusting to a lower liquid water content of L_2. As a result, the mean droplet size is reduced, as depicted in the center region of the schematic. This is what we refer to as global behavior: The boundary conditions change for a long enough time that the system is allowed to adjust to a new steady state. If data from the two steady states were to be included in the same mixing diagram, the data points would show a signature of homogeneous mixing. Thus, the question of whether the system experiences inhomogeneous or homogeneous

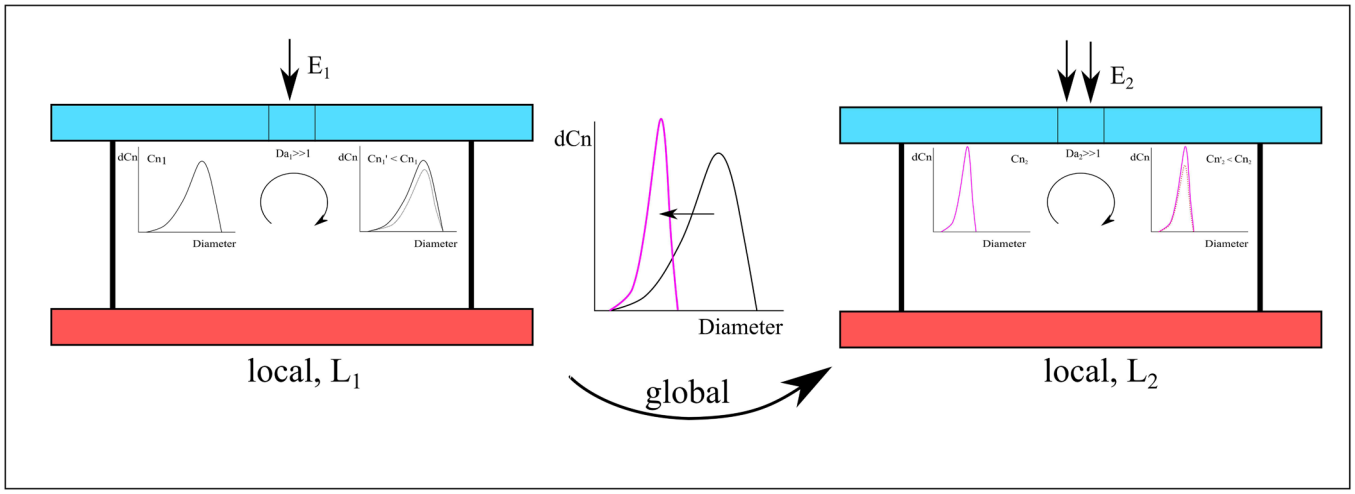

Fig. 4. Conceptual schematic of local versus global mixing signatures in the Pi Chamber. The LSC in the chamber is shown schematically between the two distributions. Under a steady state with liquid water content L_1 and entrainment E_1, the cloud droplet size distributions in upwind (solid line) and downwind (dashed line) regions of the entrainment zone are shown inside the chamber for comparison. In the entrainment region, mixing is inhomogeneous suggested by Damköhler number (Da_1); droplet number concentration is reduced, but the shape of the distribution is preserved. If the entrainment rate is then increased from E_1 to E_2, the system will come into a new steady state, with lower liquid water content (L_2). The new steady-state droplet size distribution is characterized by a shift to smaller sizes, shown in the region between the two chambers in the figure. Once the new steady state has been reached, comparison of the size distributions between the upwind and downwind regions of the entrainment zone again shows the signature of inhomogeneous mixing (Da_2).

mixing is a question of interpretation, not contradiction. Viewed locally, the mixing is always inhomogeneous, but if the system is allowed to adjust to different steady states, the mixing is effectively homogeneous. As traditionally defined, the Damköhler number captures the effect of local mixing, but not the transition between steady states. For example, in the schematic view, both Da_1 and Da_2 are much greater than unity and therefore would indicate inhomogeneous mixing.

The situation in our experiments is similar to the schematic. Note that the four groups of experiments here have the same forcing (i.e., temperature difference between top and bottom surfaces) and aerosol injection rate, while the only difference is the level of entrainment they experience (i.e., 5 LPM-20 °C, 5 LPM-30 °C, 20 LPM-20 °C, 20 LPM-30 °C). Therefore, clouds reach different steady states under different entrainment conditions (e.g., flow rate, entrained air temperature, and humidity). A cloud will have lower liquid water content and smaller droplet radius in the new steady state if it suffers more evaporation due to entrainment. The homogeneous-mixing slope of the points in Fig. 3 depends on exactly how the liquid water content adjusts in each steady state resulting from a change in the temperature or the mass flow rate of entrained air. However, in a convection-cloud chamber with constant boundary conditions and no entrainment, a shift to a smaller mean droplet diameter due to the increase of aerosol injection rate is typically associated with an increase in liquid water content due to the increased droplet residence time (e.g., refs. 28 and 29). Therefore, when entrainment is present, a shift to smaller droplet radius due to evaporation as part of the reduction of liquid water content is somewhat counteracted by this residence-time effect. Complete understanding of the slope behavior in L-D_m coordinates requires the use of more detailed models with interacting thermodynamics and microphysics.

Clouds in the atmosphere that experience more entrainment and mixing tend to have lower liquid water content, all else being equal (24). Analogous behavior can be anticipated for naturally occurring clouds in which the entrainment rate can vary substantially on length scales larger than the large-eddy scale (e.g., ~1 km). Large-scale variability at stratocumulus cloud top, for example, in different circulation regions or different shear strengths in the entrainment interfacial layer, leads to differing local steady states if it is sufficiently persistent. This is consistent with the concept of vertical circulation mixing and the associated variation in the local cloud base (14, 17). The clouds experience an organized vertical circulation initiated by the entrained and evaporatively, as well as radiatively cooled parcel. Due to the vertical circulation, the local cloud base altitude varies depending on how diluted the parcel is: higher for more diluted parcels. In some analyses of field measurements, it has been demonstrated that such variations and the resulting apparent homogeneous mixing signature can be minimized by dividing long horizontal flight paths into shorter segments (15, 17). For example, Yeom et al. (17) considered 20-s cloud segments, corresponding to 2-km long paths through stratocumulus clouds, thereby making the inhomogeneous mixing signature more clear in near-cloud-top penetrations. The transition of the mixing signature to increasingly homogeneous with increasing depth below cloud base observed there is consistent with the presence of vertical circulation and the increasing lateral mixing due to turbulent diffusion away from cloud top.

This leads to what we could consider a "homogeneous mixing paradox," further illustrated by the following scenario. Consider a stratocumulus cloud that is statistically homogeneous in the horizontal plane, with an initially uniform cloud base and a cloud top that is defined by the inversion layer at the top of the marine boundary layer. We assume that entrainment occurs at cloud top at the same global rate, but that it can occur at local rates that differ spatially and temporally, depending for example, on the local shear induced by the large-eddy circulation, etc., and we consider the following sequence of events. First, a local region of cloud with cloud base Z_1 has an adiabatic profile of liquid water content, with cloud droplet concentration N_1 and cloud-top adiabatic droplet diameter D_1, corresponding to cloud-top L_1. Then, entrainment of warm, dry air from above the inversion layer occurs, and the liquid water content is reduced to $L_2 < L_1$. We assume that the microphysical time scales are very small compared to the turbulent mixing time, such that when the mixing is complete, there is complete evaporation of some droplets to a new concentration $N_2 < N_1$, but leaving a cloud with mean droplet diameter $D_2 = D_1$. In the descending branch of the large-scale cloud circulation, the reduced liquid water content implies that

complete droplet evaporation will occur at a higher altitude and that the new cloud base is $Z_2 > Z_1$. Now, we consider the rising branch of the large-scale cloud circulation. Due to the reduced total water content, the cloud base is now $Z_3 = Z_2 > Z_1$. Presumably, the droplet concentration set at cloud base is between n_2 and n_1, due to mixing with the reservoir of aerosol particles in the boundary layer. In general, the new adiabatic profile in the updraft will have a cloud-top diameter $D_3 \neq D_1$. In fact, the entire "adiabatic" profile exhibits a different height profile of droplet diameter. This cycle is occurring continuously, but with different degrees of entrainment in each local region. If we perform a global average over the system, the mixing diagrams will appear to show homogeneous mixing, because different mean diameters occur in different cloud regions that have experienced relatively higher or lower prior entrainment. If we perform a local average, say over the region corresponding only to the initial entrainment, however, the mixing would look inhomogeneous. An important aspect of this perspective is that, in field observations, the measurements are assumed to represent the final, equilibrium mixing state, but the initial state is not known. The laboratory experiments allow the initial microphysical state of the cloud to be quantified and allow sufficient time with fixed boundary conditions so that one can be confident that a final, equilibrium state has been reached. The knowledge that multiple equilibrium states are combined in Fig. 4 enables the resolution of the homogeneous mixing paradox.

Summary and Discussion

In this work, we conduct experiments to examine the entrainment–mixing processes by injecting dry air with different temperatures and flow rates in the Pi cloud chamber. The results provide strong evidence for distinct signatures of local versus global effects of entrained air on cloud-droplet size distributions in turbulent environments. What can the idealized laboratory results tell us about entrainment–mixing processes naturally occurring near cloud top and edge in the atmosphere?

Over the past few decades, there have been tremendous efforts to understand entrainment–mixing processes in observational and modeling studies, but many challenges behind the uncertainties of entrainment-mixing studies are still unresolved. In general, the aircraft measurements for observational studies in stratocumulus clouds have flight patterns making a long horizontal penetration near the cloud top. Clouds measured over a long distance have different local environmental conditions, for example, due to different instantaneous entrainment rates. These regions, presumably of spatial extent related to the large eddy length scale, are analogous to our different experimental conditions. Within a given region, the response to entrainment and mixing can be expected to be inhomogeneous, if the microphysical conditions favor that mode; however, when averaged globally, the behavior would tend to appear as homogeneous mixing. Therefore, the local turbulence and environmental conditions control the response to the mixing process, but knowledge of the initial state and the local conditions are typically not available in an aircraft investigation. Instead, what is measured is a result of the simultaneous occurrence of different mixing stages in clouds and mixed parcels with different dilution and mixing histories that have been transported due to buoyancy differences. The results observed in this study, showing apparently contradictory inhomogeneous and homogeneous behavior, will help inform the longstanding debate about the nature of the microphysical response to mixing in clouds (e.g., refs. 8–20, 24–26, and 30–33). Specifically, the results underscore the importance of considering the scale at which measurements are made and the implications for combining multiple local equilibrium conditions when using mixing diagrams that have been the standard for data analysis since their introduction (34).

While laboratory experiments reported here were motivated by entrainment at the top of stratocumulus clouds, they reproduce atmospherically relevant ranges of the key microphysical dimensionless variables and should extend to more general scenarios (e.g., the edges of cumulus clouds): the water vapor supersaturation and the Damköhler number, with the latter depending on the droplet size distribution and the turbulent energy dissipation rate. Of course, experiment parameters related to the large-scale flow do not match those in natural clouds, such as the turbulence Reynolds number and the Richardson number, which is relevant to shear versus buoyancy driving of the entrainment process (35). Recent theoretical work, however, is in agreement on the key roles of the microphysical dimensionless variables in determining whether a cloud undergoing entrainment exhibits homogeneous or inhomogeneous mixing, and we discuss next how this helps connect to the atmospheric context.

Jeffery (30) and Lehmann et al. (8) both drew attention to the fact that two time scales govern the microphysical response to mixing: the single-droplet evaporation time and the phase relaxation time (the supersaturation response time). Pinsky et al. (31) expressed the mixing problem in terms of dimensionless variables Da and a potential evaporation parameter that depends on the clear-air humidity. The resulting dimensionless space is depicted in their figure 16. Their results show that the inhomogeneous mixing limit is achieved for $Da \gg 1$ and a potential evaporation parameter approaching zero. They only consider the case of mixing of equal mass fractions of cloudy and clear air. Our understanding is that the potential evaporation parameter effectively becomes even smaller in magnitude when the mass fraction of clear air is reduced, such as in our experiments. We therefore expect that our observation of local inhomogeneous mixing is consistent with the dimensionless space (31). Fries et al. (32) nondimensionalize the governing equations and determine that three variables govern the microphysical evolution in response to entrainment: a Damköhler number involving the phase relaxation time, denoted as Da_s, a Damköhler number involving the droplet evaporation time, denoted as Da_d, and a cloud mixing fraction. They point out that the potential evaporation parameter of Pinsky et al. (31) is equivalent to the ratio of the two Damköhler numbers. They depict the resulting dimensionless space in their Fig. 4 (Da_d/Da_s relative to a critical ratio depending on the cloud mixing fraction, versus Da_d). Inhomogeneous mixing is favored for large Da_d and for Damköhler ratio approaching the critical value, i.e., nearing complete evaporation. Our observations appear to be consistent with the mapping of the inhomogeneous region within the dimensionless space (32). More quantitative comparison with numerical simulations and theoretical analysis will be helpful, but for now, we can conclude that the experiments presented here lie within atmospherically relevant microphysical dimensionless parameter space and are at least qualitatively consistent with the predicted regimes for inhomogeneous mixing.

The results reported here provide physically based evidence for the microphysical effects of the entrainment–mixing process. The local effects of entrainment are evident when we compare the droplet size distributions in the upwind, center, and downwind regions for the same entrained air conditions (flow rate, temperature, and humidity). Cn and L in the downwind region decrease significantly, but the difference in D_m between the three regions is small. Such behavior is consistent with the inhomogeneous mixing scenario expected from the analysis of time scales. However, from the system, or global, point of view, decreases in

Cn, L, and D_m are observed as entrainment conditions T_e and Q_e increase. When results from different entrainment conditions are combined, a signature emerges that is consistent with homogeneous mixing. The apparent contradiction is understood as the cloud microphysical responses to entrainment and mixing differing on local and global scales: locally inhomogeneous and globally homogeneous. While clearly more complex than the laboratory, we can consider as a conceptual picture that each large eddy or circulating region within a stratocumulus cloud can be considered as its own cloud-chamber experiment, with a corresponding entrainment rate and local equilibrium value of liquid water content (as in Fig. 4). The local Damköhler number in each region is likely to be very large compared to unity, and therefore the local mixing signatures will be predominantly inhomogeneous. When ensemble averaged over many of these large eddies or circulation regions, however, the resulting microphysical signature will indicate homogeneous mixing. The apparent inconsistency suggests that great care should be taken in interpreting measurements, and perhaps even that the classical picture of inhomogeneous versus homogeneous mixing needs to be revised to account for the large-scale variability that is an inherent part of even the most uniform clouds, such as statistically homogeneous stratocumulus. Finally, in the real atmosphere, the entrainment–mixing process would occur differently depending on the RH of entrained air and the local rate of entrainment, and becomes more complicated when we consider aerosols in entrained air (e.g., secondary droplet activation). Therefore, this work is just a first step in investigations of the effects of entrainment–mixing processes, and further research is planned.

Data, Materials, and Software Availability. Data required to reproduce figures have been deposited in Digital Commons (10.37099/mtu.dc.all-datasets/42) (36).

ACKNOWLEDGMENTS. This work was supported by Department of Energy Office of Science grant number DE-SC0022128. F.Y. was supported by the Office of Biological and Environmental Research in the Department of Energy, Office of Science, through the United States Department of Energy Contract No. DE-SC0012704 to Brookhaven National Laboratory.

1. J. Latham, R. L. Reed, Laboratory studies of the effects of mixing on the evolution of cloud droplet spectra. *Q. J. R. Meteorol. Soc.* **103**, 297–306 (1997).
2. S. S. Shy, R. E. Breidenthal, Laboratory experiments on the cloud-top entrainment instability. *J. Fluid Mech.* **214**, 1–15 (1990).
3. S. S. Shy, R. E. Breidenthal, Turbulent stratified interfaces. *Phys. Fluids A* **3**, 1278–1285 (1991).
4. D. A. Randall, Conditional instability of the first kind upside-down. *J. Atmos. Sci.* **37**, 125–130 (1980).
5. J. W. Deardorff, Cloud top entrainment instability. *J. Atmos. Sci.* **37**, 131–147 (1980).
6. S. T. Siems, C. S. Bretherton, M. B. Baker, S. Shy, R. E. Breidenthal, Buoyancy reversal and cloud-top entrainment instability. *Q. J. R. Meteorol. Soc.* **116**, 705–739 (1990).
7. B. J. Sayler, R. E. Breidenthal, Laboratory simulations of radiatively induced entrainment in stratiform clouds. *J. Geophys. Res. Atmos.* **103**, 8827–8837 (1998).
8. K. H. Lehmann, H. Siebert, R. A. Shaw, Homogeneous and inhomogeneous mixing in cumulus clouds: Dependence on local turbulence structure. *J. Atmos. Sci.* **66**, 3641–3659 (2009).
9. J. Wang *et al.*, Observations of marine stratocumulus microphysics and implications for processes controlling droplet spectra: Results from the marine stratus/stratocumulus experiment. *J. Geophys. Res.* **114**, D18210 (2009).
10. C. Lu, Y. Liu, S. Niu, Examination of turbulent entrainment-mixing mechanisms using a combined approach. *J. Geophys. Res.* **116**, D20207 (2011).
11. C. Lu, Y. Liu, S. Niu, S. Endo, Scale dependence of entrainment-mixing mechanisms in cumulus clouds. *J. Geophys. Res. Atmos.* **119**, 13,877–13,890 (2014).
12. M. H. Tölle, S. K. Krueger, Effects of entrainment and mixing on droplet size distributions in warm cumulus clouds. *J. Adv. Model. Earth Sys.* **6**, 281–299 (2014).
13. M. J. Beals *et al.*, Holographic measurements of inhomogeneous cloud mixing at the centimeter scale. *Science* **350**, 87–90 (2015).
14. S. S. Yum *et al.*, Cloud microphysical relationships and their implication on entrainment and mixing mechanism for the stratocumulus clouds measured during the VOCALS project. *J. Geophys. Res. Atmos.* **120**, 5047–5069 (2015).
15. J. M. Yeom, S. S. Yum, Y. Liu, C. Lu, A study on the entrainment and mixing process in the continental stratocumulus clouds measured during the RACORO campaign. *Atmos. Res.* **194**, 89–99 (2017).
16. N. Desai, S. Glienke, J. P. Fugal, R. A. Shaw, Search for microphysical signatures of stochastic condensation in marine boundary layer clouds using airborne digital holography. *J. Geophys. Res. Atmos.* **124**, 2739–2752 (2019).
17. J. M. Yeom *et al.*, Vertical variations of cloud microphysical relationships in marine stratocumulus clouds observed during the ACE-ENA campaign. *J. Geophys. Res. Atmos.* **126**, e2021JD034700 (2021).
18. F. Hoffmann, G. Feingold, Entrainment and mixing in stratocumulus: Effects of a new explicit subgrid-scale scheme for large-eddy simulations with particle-based microphysics. *J. Atmos. Sci.* **76**, 1955–1973 (2019).
19. S. K. Krueger, Linear eddy modeling of entrainment and mixing in stratus clouds. *J. Atmos. Sci.* **50**, 3078–3090 (1993).
20. D. Niedermeier *et al.*, Observation of a link between energy dissipation rate and oscillation frequency of the large-scale circulation in dry and moist Rayleigh–Bénard turbulence. *Phys. Rev. Fluids* **3**, 501 (2018).
21. J. C. Anderson, S. Thomas, P. Prabhakaran, R. A. Shaw, W. Cantrell, Effects of the large-scale circulation on temperature and water vapor distributions in the Π Chamber. *Atmos. Meas. Tech.* **14**, 5473–5485 (2021).
22. K. Chang *et al.*, A laboratory facility to study gas–aerosol–cloud interactions in a turbulent environment: The Π Chamber. *Bull. Am. Meteorol. Soc.* **97**, 2343–2358 (2016).
23. I. Faloona *et al.*, Observations of entrainment in eastern Pacific marine stratocumulus using three conserved scalars. *J. Atmos. Sci.* **62**, 3268–3285 (2005).
24. H. Gerber *et al.*, Entrainment rates and microphysics in POST stratocumulus. *J. Geophys. Res. Atmos.* **118**, 12,094–12,109 (2013).
25. M. B. Baker, R. G. Corbin, J. Latham, The influence of entrainment on the evolution of cloud-droplet spectra: I. A model of inhomogeneous mixing. *Q. J. R. Meteorol. Soc.* **106**, 581–598 (1980).
26. F. Burnet, J. L. Brenguier, Observational study of the entrainment-mixing process in warm convective clouds. *J. Atmos. Sci.* **64**, 1995–2011 (2007).
27. K. K. Chandrakar *et al.*, Aerosol indirect effect from turbulence-induced broadening of cloud-droplet size distributions. *Proc. Natl. Acad. Sci. U.S.A.* **113**, 14243–14248 (2016).
28. S. Thomas, F. Yang, M. Ovchinnikov, W. Cantrell, R. A. Shaw, Scaling of turbulence and microphysics in a convection–cloud chamber of varying height. *J. Adv. Model. Earth Syst.* **15**, e2022MS003304 (2023).
29. S. K. Krueger, Equilibrium droplet size distributions in a turbulent cloud chamber with uniform supersaturation. *Atmos. Chem. Phys.* **20**, 7895–7909 (2020).
30. C. A. Jeffery, Inhomogeneous cloud evaporation, invariance, and Damköhler number. *J. Geophys. Res. Atmos.* **112**, D24S21 (2007).
31. M. Pinsky, A. Khain, A. Korolev, Theoretical analysis of mixing in liquid clouds–Part 3: Inhomogeneous mixing. *Atmos. Chem. Phys.* **16**, 9273–9297 (2016).
32. J. Fries, G. Sardina, G. Svensson, B. Mehlig, Key parameters for droplet evaporation and mixing at the cloud edge. *Q. J. R. Meteorol. Soc.* **147**, 2160–2172 (2021).
33. C. Lu *et al.*, On which microphysical time scales to use in studies of entrainment-mixing mechanisms in clouds. *J. Geophys. Res. Atmos.* **123**, 3740–3756 (2018).
34. J. B. Jensen, P. H. Austin, M. B. Baker, A. M. Blyth, Turbulent mixing, spectral evolution and dynamics in a warm cumulus cloud. *J. Atmos. Sci.* **42**, 173–192 (1985).
35. J. Katzwinkel, H. Siebert, R. A. Shaw, Observation of a self-limiting, shear-induced turbulent inversion layer above marine stratocumulus. *Bound. Layer Meteorol.* **145**, 131–143 (2012).
36. J. Yeom *et al.*, Cloud microphysical response to entrainment and mixing is locally inhomogeneous and globally homogeneous: Evidence from the lab. Digital Commons. http://doi.org/10.37099/mtu.dc.all-datasets/42. Deposited 28 April 2023.